Supporting Online Material for:

Planarian Hh signaling regulates regeneration polarity and links Hh pathway evolution to cilia

Jochen C. Rink*, Kyle A. Gurley*, Sarah A. Elliott, Alejandro Sánchez Alvarado¶

*: Authors contributed equally to this work

¶ To whom correspondence should be addressed: sanchez@neuro.utah.edu

Department of Neurobiology & Anatomy

Howard Hughes Medical Institute

University of Utah School of Medicine

401 MREB, 20 North 1900 East

Salt Lake City, UT 84103

Supporting Online Materials:

MATERIALS AND METHODS

In Situ Hybridization and antibody staining. Animals were killed, fixed, hybridized, and developed as previously described (*1*). Following development with NBT/BCIP, animals were incubated in anti-α-tubulin antibody (1:300, NeoMarkers) to detect the CNS and pharynx, anti-phospho-histone-H3 (1:200, Zymax) to detect mitotic activity, or anti-acetylated tubulin (1:300, Sigma) to label cilia. Primary antibodies were detected with alexa-fluor-488, -555, or -647 anti-Mouse or anti-Rabbit secondary antibodies (1:600; Invitrogen). In some cases, following NBT/BCIP development to detect the first Dig-labeled riboprobe, a second riboprobe labeled with 2,4-dinitrophenol (DNP) was detected using an HRP-conjugated anti-DNP antibody (1:100, PerkinElmer) and tyramide signal amplification. For confocal imaging, animals were mounted in 2:1 Benzyl benzoate:Benzyl alcohol after dehydration in Methanol.

Gene identification and cloning. Human and *Drosophila* protein sequences were used to find planarian homologs from the *S. mediterranea* genome database via BLAST. Planarian homologs were then used for reciprocal BLAST against the human refseq database to verify homology. Protein domains were predicted using InterPro (*2*). All sequences were cloned from cDNA obtained from an 8-day regeneration series as described (*3*). Full-length cDNA sequences for *hh*, *ptc*, *smo, sufu*, *gli-1, gli-2,* and *gli-3* were obtained using 5' RACE (Generacer, Invitrogen) and 3' RACE. *iguana* cDNA was provided by EST NBE.7.10A (GenBank: AY967686).

Primers used for cloning the remaining genes.

F *fu: ATGGATAAATACCACGTACTTGAAC*

R *fu: poly-T*

F *kif27: CATGCATTAGAGTATCACCGGAT*

R *kif27: CGAATGTTACGAGCTCTGTTGG*

F *IFT172: TACTCATCCAAGTGCTCCTTATGC*

R *IFT172: AACTGCTTGCCTGTAGAAACTTCC*

F *IFT88: AAACCAGTTACGGTCGCAAG*

R *IFT88: GCAGTTTTCGGTCTTTCAGC*

F *IFT52: TGCTACATTGAGAGTGGAGGATCG*

R *IFT52: TCATACGACTCAAGAGCCTTTGG*

F *Kif3B: AGAAGGACCAAGGCGATTTAC*

R *Kif3B: TCAGCCTCATGTTCTTGTCG*

F *ndk:* GCACAATACCGATTGTCAAACCCT

R *ndk:* GGCTTGATAATGGCTAACTGGT

F *ndl-3:* TTATTGACAGTAGGAACCAAAGCC

R *ndl-3:* ATCCTGAATCAAGTCAACGCCA

F *ndl-4:* ACCAAAGCAATCCAACTGCC

R *ndl-4:* GAAGGCGACGACGAATTTTGTCCTGG

RNAi via dsRNA feeding. Gene silencing was performed as previously described using SOFT SERVE (*3*). To increase the ratio of dsRNA-containing bacteria to liver paste, 50 ml of IPTG-induced bacterial culture was pelleted and mixed with 125 µl liver paste (2 parts liver: 1 part water). For simultaneous silencing of two genes, 25 ml of each IPTG-induced culture was mixed prior to pelleting to make 50 ml of total culture. Feeding and amputation schedules were tailored for each experiment and are described in the figure legends.

Fig 1B 16 dsRNA feedings over 2 months

Fig 1C 3 dsRNA feedings

Fig 2 A-F	3 dsRNA feedings prior to amputation
Fig 3A	3 dsRNA feedings prior to amputation. All food is mixed for all feeds such that each *gene(RNAi)* is diluted 50%
Fig 3B	6 feedings of control(RNAi) or *ptc(RNAi)* at 100% dose, followed by a single feeding of *βcatenin-1(RNAi)* or control(RNAi).
Fig 3C	Top row, 9 dsRNA feedings. Bottom row, 3 dsRNA feedings
Fig 3D,E	7 dsRNA feedings prior to amputation
Fig 4A-E	3 dsRNA feedings prior to amputation/14d regeneration, 3 dsRNA feedings
Sup. 5	9 dsRNA feedings
Sup. 6	Top panel, 3 dsRNA feedings prior to amputation/14d regeneration, 3 dsRNA feedings. Bottom panel, No dsRNA feedings.
Sup. 7	3 dsRNA feedings
Sup. 8	6 dsRNA feedings
Sup. 9	3 dsRNA feedings prior to amputation
Sup. 10	Two sets of three RNAi-feedings interrupted by one round amputation/regeneration.
Sup. 11	9 dsRNA feedings prior to amputation
Sup. 12	3 dsRNA feedings diluted 50% with control(RNAi)
Sup. 13	Top panel, 9 dsRNA feedings. Bottom panel, 3 dsRNA feedings
Sup. 14	Top row, 3 dsRNA feedings. Bottom row, 6 dsRNA feedings
Sup. 15	9 dsRNA feedings
Sup. 16	6 dsRNA feedings
Sup. 20	A, 6 dsRNA feedings. B, 9 dsRNA feedings.
Sup. 18, 19, 21	3 dsRNA feedings prior to amputation/14d regeneration, 3 dsRNA feedings. For *in situ*-hybridizations in 19 and 21, animals were amputated after the 2nd round of feedings.

Imaging and image quantification. A Zeiss Lumar V12 equipped with an Axiocam HRc was used to capture live images, movies and epi-fluorescence images. A Zeiss LSM510-live was used for confocal imaging and image projections. The image analysis software package Kalaimoscope (*4*) (Transinsight GmBH) was used to quantify H3P-density in epi-fluorescence images and movement speed from movie sequences (120 frames acquired at 2.5 Hz). Translocation velocity was defined as the average rate of centroid translocation between successive frames.

Supplemental Fig. 1

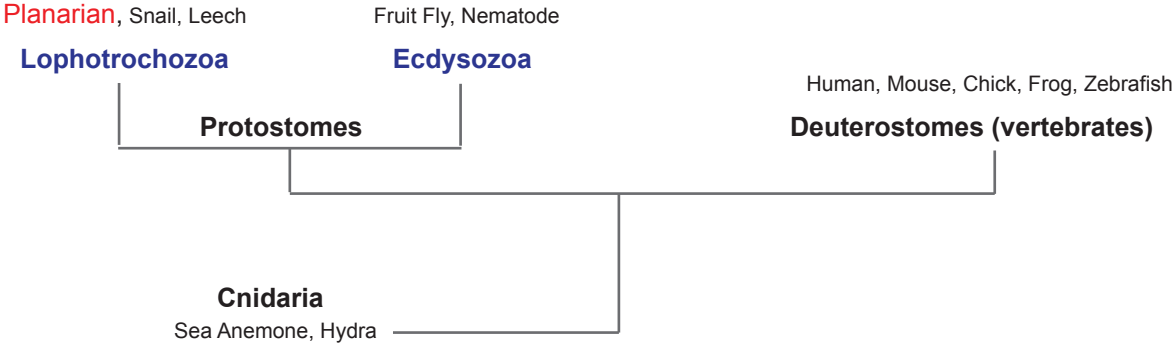

Supplemental Fig. 2

A

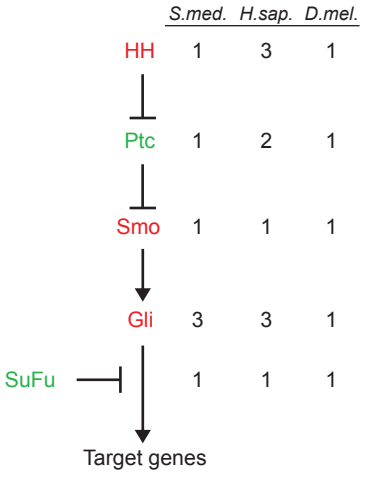

B

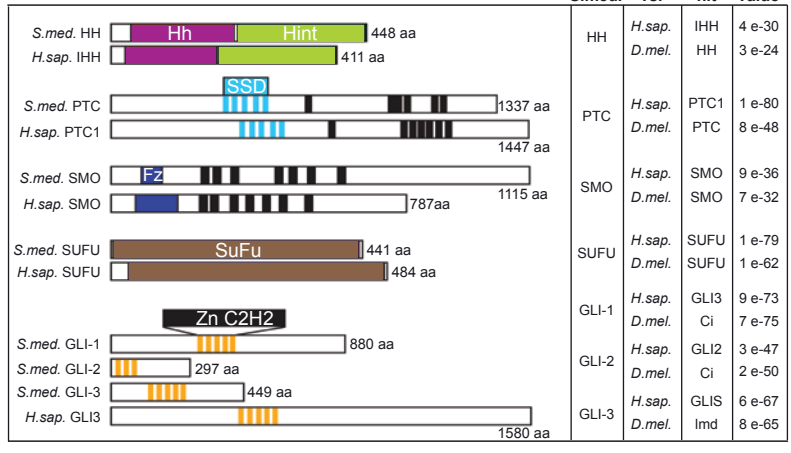

S.med.	vs.	Best hit	E value
HH	*H.sap.*	IHH	4 e-30
	D.mel.	HH	3 e-24
PTC	*H.sap.*	PTC1	1 e-80
	D.mel.	PTC	8 e-48
SMO	*H.sap.*	SMO	9 e-36
	D.mel.	SMO	7 e-32
SUFU	*H.sap.*	SUFU	1 e-79
	D.mel.	SUFU	1 e-62
GLI-1	*H.sap.*	GLI3	9 e-73
	D.mel.	Ci	7 e-75
GLI-2	*H.sap.*	GLI2	3 e-47
	D.mel.	Ci	2 e-50
GLI-3	*H.sap.*	GLIS	6 e-67
	D.mel.	lmd	8 e-65

Supplemental Fig. 3

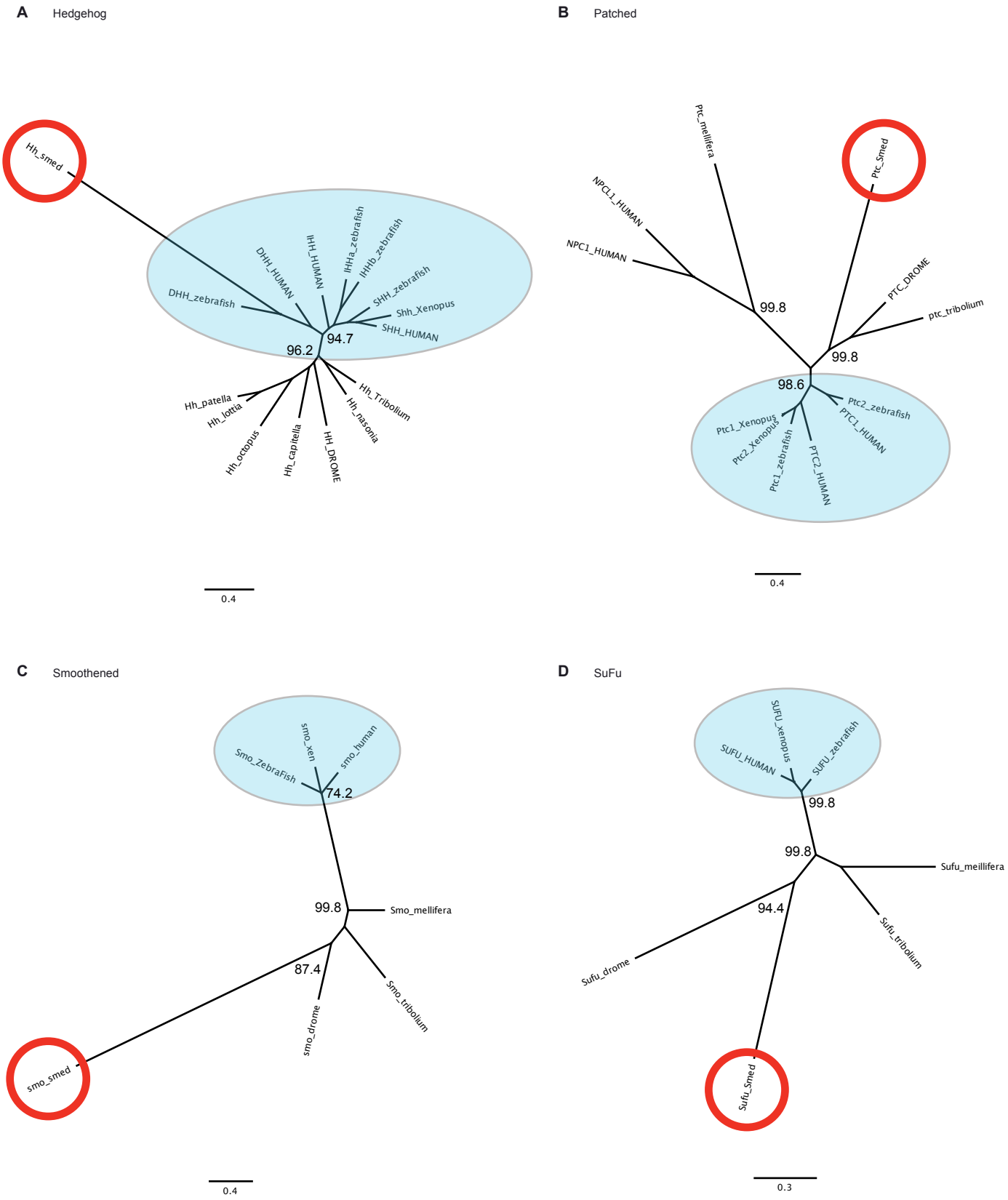

Supplemental Fig. 4

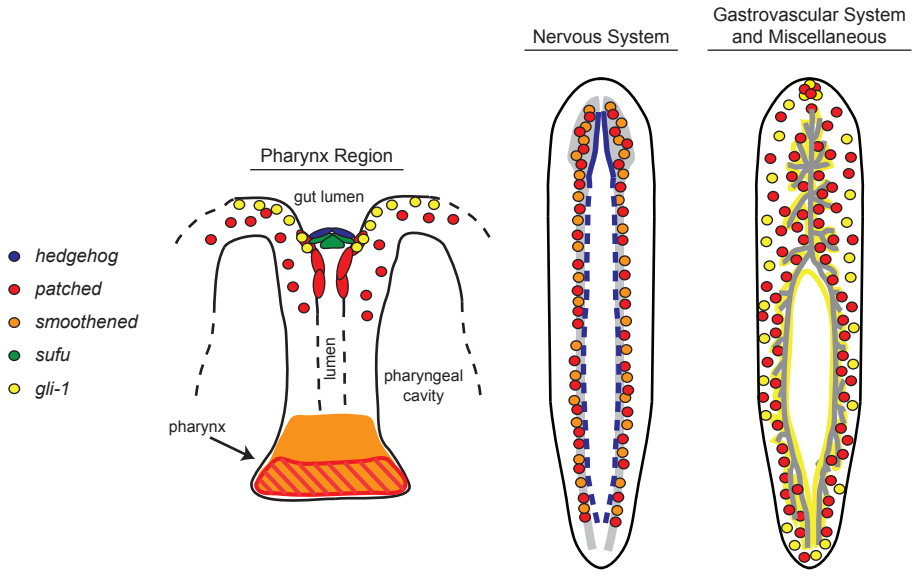

Supplemental Fig. 5

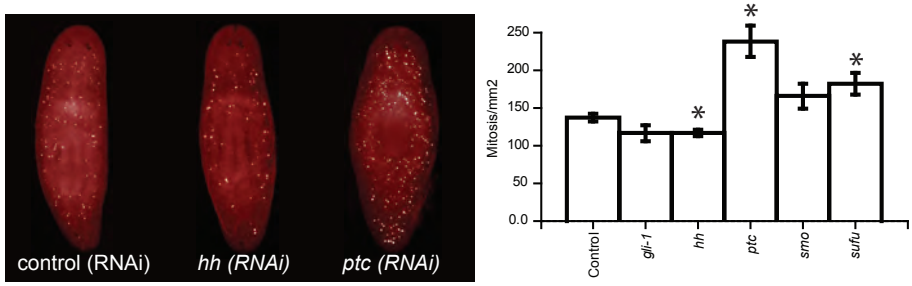

Supplemental Fig. 6

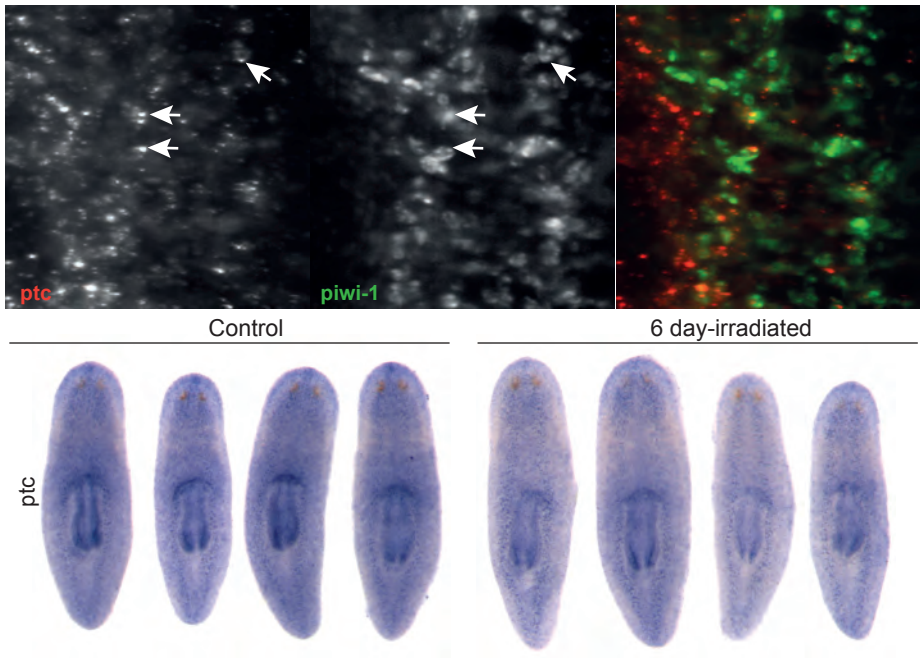

Supplemental Fig. 7

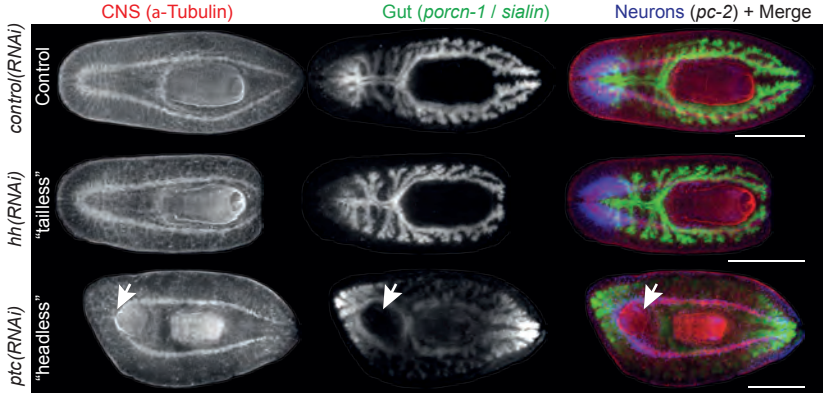

Supplemental Fig. 8

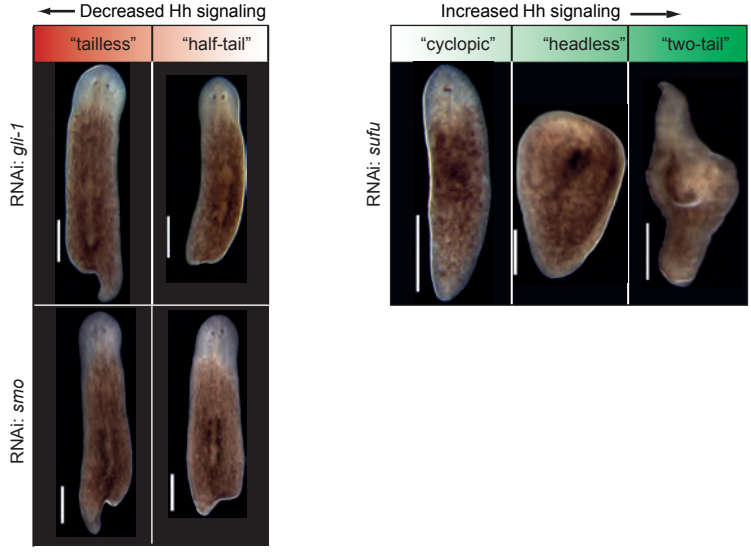

Supplemental Fig. 9

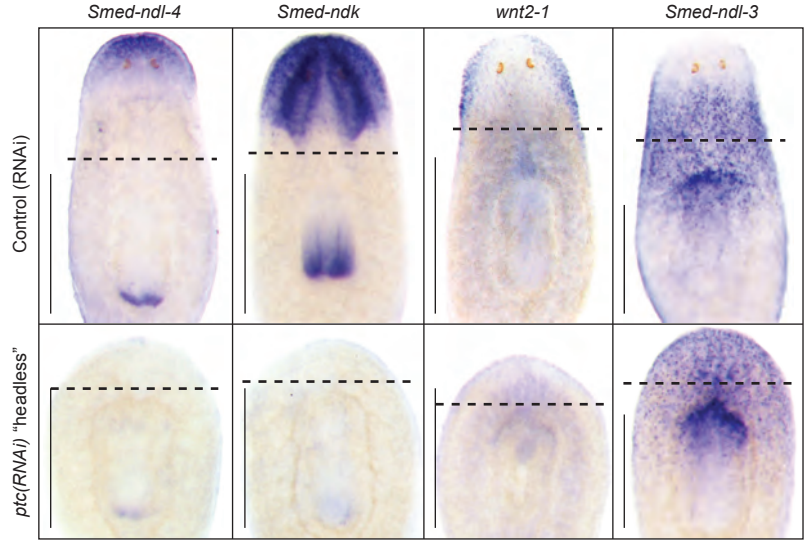

Supplemental Fig. 10

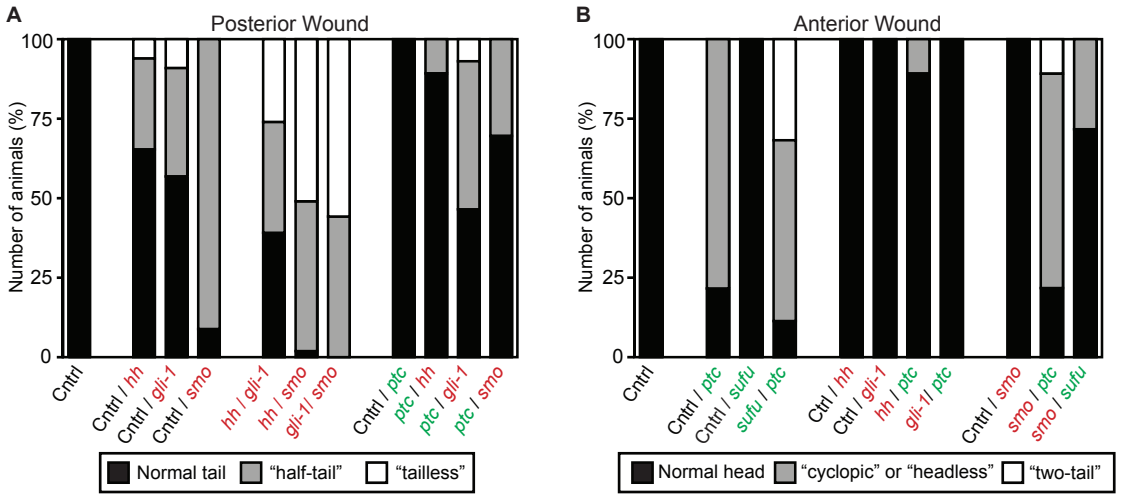

Supplemental Fig. 11

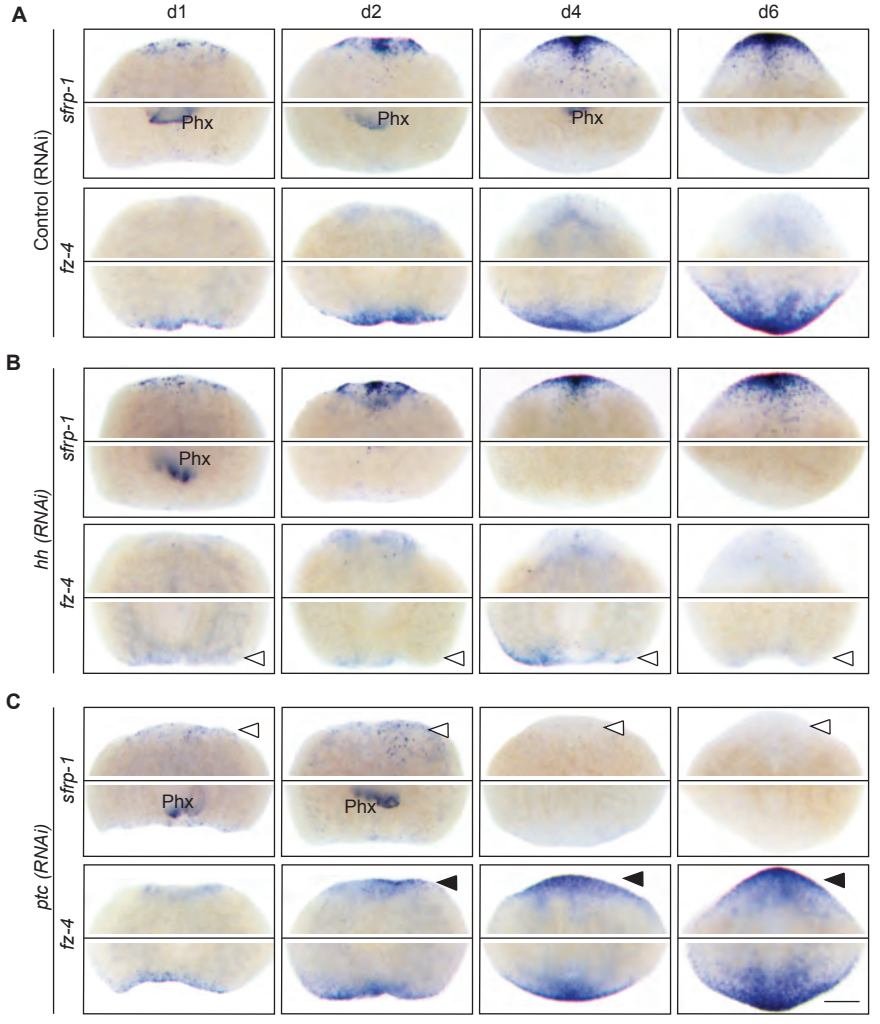

Supplemental Fig. 12

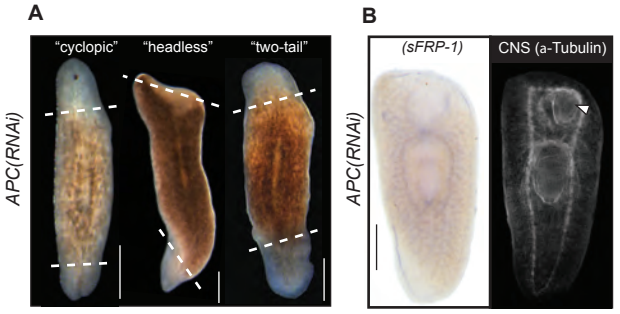

Supplemental Fig. 13

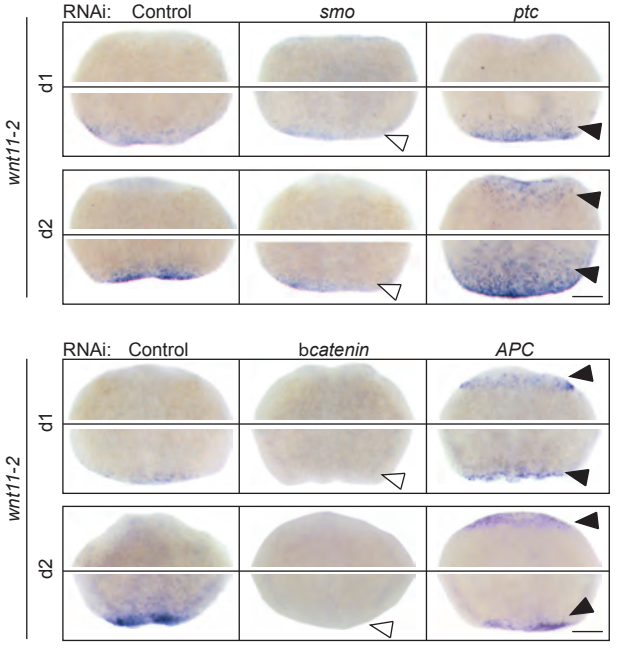

Supplemental Fig. 14

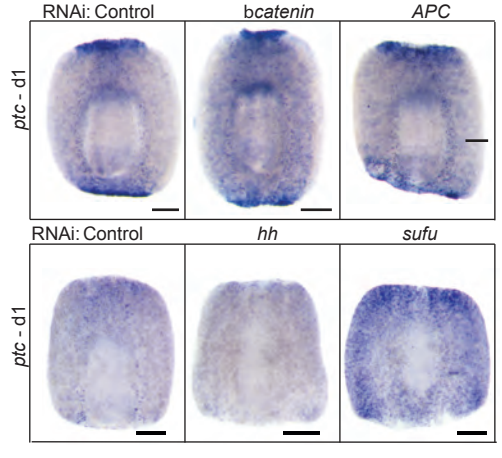

Supplemental Fig. 15

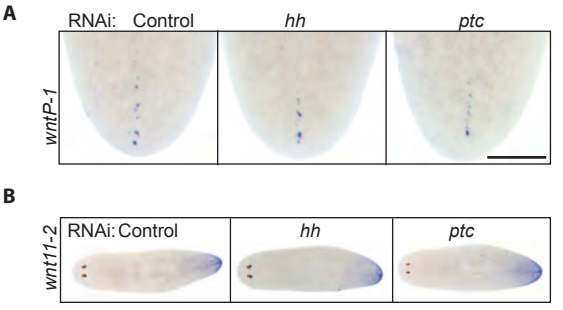

Supplemental Fig. 16

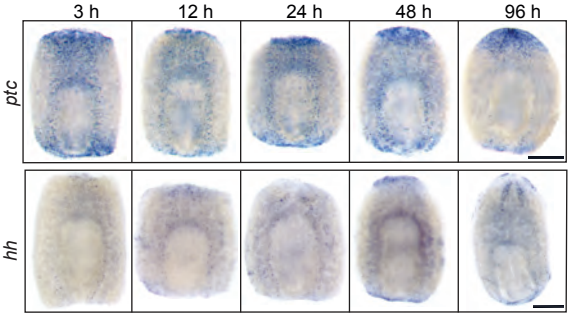

Supplemental Fig. 17

	S.med. query vs *H.s.*		*S.med.* query vs *D.m.*		*D.m.* query vs *H.s.*	
SMED-sequence	***H.s.* best hit**	**E-value**	***D.m.* best hit**	**E-value**	***H.s.* best hit**	**E-value**
SMED-IFT52	IFT52	2.00E-70	osm-6	7.00E-46	IFT52	1.00E-77
SMED-IFT88f	IFT88	3.00E-94	nompB	1.00E-45	IFT88	2.00E-98
SMED-IFT88r	IFT88	8.00E-89	nompB	3.00E-19	IFT88	2.00E-98
SMED-IFT172f	IFT172	2.00E-120	osm-1	2.00E-88	IFT172	0.00E+00
SMED-IFT172r	IFT172	2.00E-59	osm-1	3.00E-36	IFT172	0.00E+00
SMED-DNAH-b1	DNAH9	0.00E+00	Dyn. HC at 93AB	0.00E+00	DNAH17	0.00E+00
SMED-FUSED	STK36, Fused	3.00E-118	fused	1.00E-79	STK36, Fused	2.00E-84
SMED-KIF27	Kif27	2.00E-102	Klp31E	7.00E-75	Kif21B	0.00E+00
SMED-KIF3B	Kif3B	0.00E+00	Klp68D	1.00E-120	Kif3B	2.00E-168

Supplemental Fig. 18

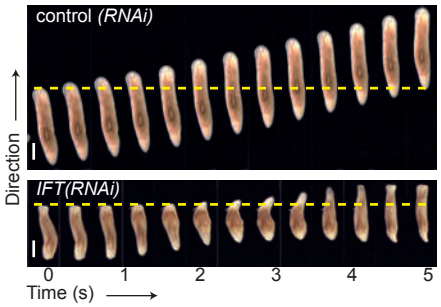

Supplemental Fig. 19

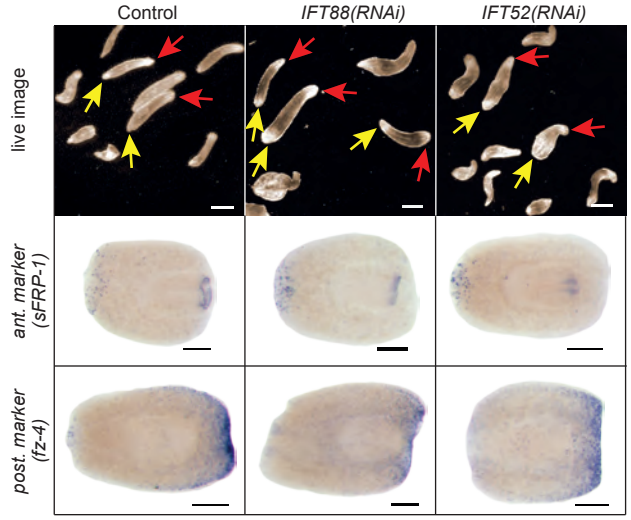

Supplemental Fig. 20

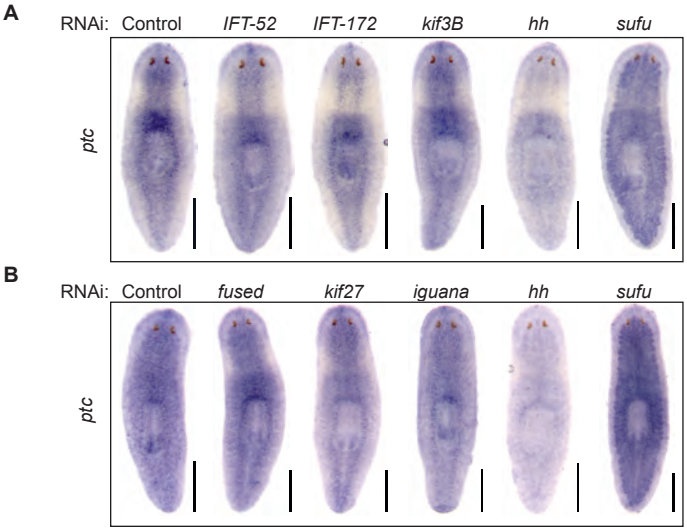

Supplemental Fig. 21

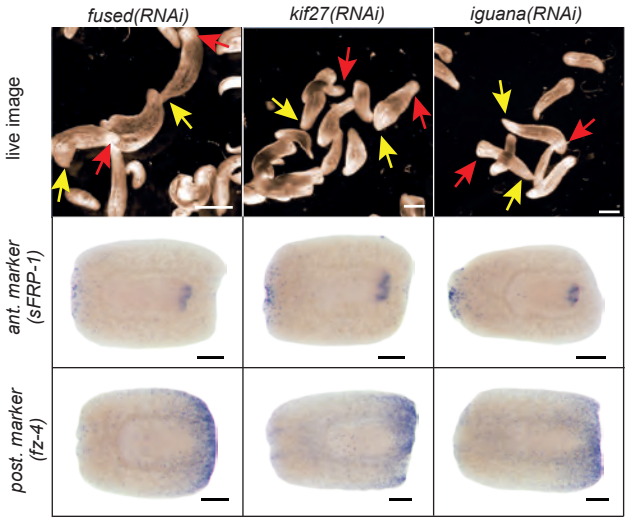

Supplemental Fig. 22

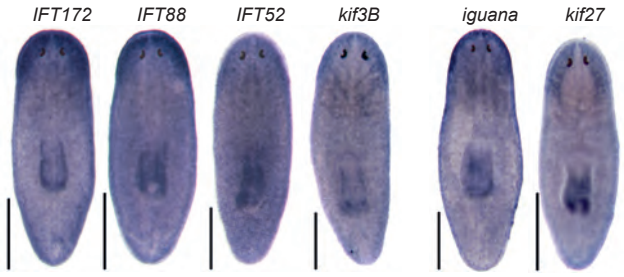

Supplemental Fig. 23

planaria

Hh pathway

Kif27 / Fused — IFT / cilia

Iguana = cilia

fruit fly

Hh pathway

Cos2 / Fused ? IFT / cilia

Iguana = ?

zebrafish

Hh pathway

Kif7 / Fused — IFT / cilia

Iguana = Hh + cilia

mice

Hh pathway

Kif7

Kif27 / Fused — IFT / cilia

Iguana = ?

Protostomes

Deuterostomes

Hh pathway

Cos2/Kif27/Kif7 Fused — IFT / cilia

SUPPLEMENTAL FIGURE LEGENDS AND NOTES

Figure S1. Schematic illustrating the phylogenetic position of planarians (*5, 6*). As part of the lophotrochozoans, a sister clade to the ecdysozoa, planarians are a useful model organism to investigate the evolution of all bilaterians. Features shared by planarians and vertebrates (deuterostomes) were likely to be present in the common bilaterian ancestor.

Figure S2. (**A)** Schematic of core component function in the Hh pathway. Negative and positive interactions are symbolized by T-bars and arrows, respectively. Red, activators - RNAi decreases signaling. Green, inhibitors - RNAi increases signaling. The number of core component homologs in *Schmidtea mediterranea*, *Homo sapiens* and *Drosophila melanogaster* are indicated. (**B)** Homology analysis of planarian Hh components. Domains found by InterPro (*2*) for planarian and human proteins. Best reciprocal BLAST hits in human and fly refseq protein database. Hint, Intein domain. SSD, Sterol Sensing Domain. Fz, Frizzled. SuFu, Supressor of Fused. Zn_C2H2, zinc finger domain subfamily. Black/light-blue bars, trans-membrane domains. Planarian sequences nomenclature (Gli-1, Gli-2, and Gli-3) does not reflect direct orthology to the mammalian counterparts.

Figure S3. Phylogenetic tree inferred from TCoffee alignment of full-length proteins. Bayesian analysis was implemented in Geneious using the MrBayes Plugin (*7*). Confidence values are indicated at selected nodes and scale bars represent the average number of substitutions per site. **(A)** Surprisingly, SMED-HH clusters with vertebrate sequences instead of the protostome sequences. However, this is likely an artifact of the extremely long branch length, indicating the planarian HH protein is quite divergent. **(B)** SMED-PTC clusters preferentially with protostome sequences over vertebrate sequences. NPC proteins are related to the PTC proteins. **(C)** SMED-SMO clusters preferentially with protostome sequences over vertebrate sequences. Note the long

planarian branch length. **(D)** SMED-SUFU clusters preferentially with protostome sequences over vertebrate sequences.

Figure S4. Schematic of core component expression patterns, color coding as indicated. Anterior, Top. Posterior, Bottom. (**Left)** The pharynx. Top, Close-up of the connection between pharynx and gut (root of the pharynx). Expression of *hh*, *ptc*, *sufu* and *gli1* in complex, partially overlapping patterns. Bottom, *ptc* and *smo* are further prominently expressed in the distal aspects of the pharynx. (**Center)** The planarian central nervous system (CNS, gray), comprising the bi-lobed brain and two ventral nerve cords (VNC) running the length of the animal. *hh* is expressed along the medial boundary of the brain lobes and faintly along the VNC. *smo* and *ptc* are expressed within the brain and along the length of the VNC. (**Right**) The planarian gastrovascular system (gray). *gli1* is prominently expressed in a layer of cells surrounding the gut enterocytes. *ptc* is expressed in a similar pattern, faintly in control animals, but very prominently upon upregulation of Hh signaling. These data could indicate that the cells surrounding the gut enterocytes normally respond to Hh signals. However, *hh* was not detected within the gastrovascular system, which is likely due to sub-optimal sensitivity of *hh in situ* hybridization (see below). In addition to their gastrovascular expression domains, both *ptc* and *gli1* are strongly expressed in cells scattered throughout the animal, which are enriched along the ventral lateral margins and along the anterior-most section of the midline. Note: Only conspicuous aspects of individual expression patterns were depicted in this figure. Diffuse staining with *ptc*, *smo*, and *sufu* probes suggests wide-spread expression in many tissues. The strong *gli-1*signal in the gastrovasculature and in scattered superficial cells may obscure further sites of expression (e.g., brain, CNS). The *hh* probe is very weak and likely capable only of detecting high levels of *hh* expression. Therefore, the medial boundary of the brain, the VNC and the base of the pharynx likely constitute strong sources of HH ligand.

Figure S5. Hh pathway activity affects planarian cell division. **Top**, Quantification of mitotic density in RNAi-treated intact animals. Mitotic cells were visualized with anti-phospho-Histone H3 (H3P). n > 8 animals/condition. Error bars, SEM. Asterisks: p-value < 0.005 vs. control (Student's T-test). The fact that the *gli-1(RNAi) or smo(RNAi)*-induced changes were not statistically significant in this experiment is likely due to the limited sample size. **Bottom**, whole mount stain visualizing mitotic cells (anti-H3P) of representative animals. Scale bars, 0.5 mm.

Figure S6. *ptc* is expressed in subset of stem cells. **(Top)** Double fluorescent whole-mount *in situ* hybridization for *ptc* (left) and stem cell marker *Smed-piwi-1* (middle) and Merge (right). *ptc* expression was increased by *sufu*(RNAi). Arrows, cells double-positive for *piwi* and *ptc*. Scale bar, 50 μm. (**Bottom)** *ptc* expression in control animals and animals irradiated six days prior to fixation to remove stem cells. 4 examples of each condition are shown to illustrate staining consistency. The fact that *ptc* expression is largely unaffected by depletion of *piwi-1*-positive stem cells is consistent with the minor overlap between *ptc* and *piwi-1* (top). *piwi-1*-positive cells account for the majority of planarian cell divisions and therefore represent the most likely target of mitogenic Hh signaling. Because of the low degree of ptc/piwi coexpression, we currently cannot distinguish between direct and indirect effects of Hh on planarian stem cells.

Figure S7. Gut and CNS-anatomy in "Tailless" and "Headless" animals. Trunk fragments of dsRNA-fed animals 14 days after amputation. Anatomical stains on indicated phenotype categories. CNS-staining (α-Tubulin antibody, left), Gut (*Smed-porcn*-1 and *Smed-sialin* riboprobes, center) and Merge (right, also including the neuronal marker *pc-2* (blue)). Arrows mark ectopic pharynx (left) and pharyngeal cavity (center). Images are confocal projections. Scale bar, 0.5 mm.

Figure S8. Phenotypic consistency amongst Hh pathway activators or inhibitors. *gli-1(RNAi)* and *smo(RNAi)* recapitulate *hh(RNAi)* tail regeneration defects (Fig.2); *sufu(RNAi)* recapitulates the

spectrum of anterior regeneration defects caused by *ptc(RNAi)* (Fig. 2). Regenerating trunk fragments (*gli-1, smo*) or tail fragments (*sufu*) were imaged 18 days after amputation. *sufu(RNAi)* causes the same anterior regeneration phenotypes in trunk fragments, but for unknown reasons, phenotypic penetrance is higher in tail fragments.

Figure S9. Marker panel (*Smed-noudarake-like-4* (*ndl-4*)*, Smed-noudarake* (*ndk*)*, Smed-noudarake-like-3* (*ndl-3*) with graded A/P expression domains in control(RNAi) and "headless" *ptc(RNAi)* animals. Dotted lines, amputation plane. Scale bars, 0.5 mm. Expression of *ndl-3* indicates that the regenerated tissue is not devoid of A/P-patterning information even though markers for the most anterior fates are not expressed.

Figure S10. Double-RNAi experiments to probe functional synergy between Hh pathway genes. Quantification of double-RNAi experiments, depicting relative frequency of the indicated phenotypes in a cohort of trunk fragments at **(A)** posterior and **(B)** anterior amputation sites. RNAi of red genes leads to decreased signaling and RNAi of green genes leads to increased signaling. Animals were scored 14 days after amputation. Data is from two independent experiments, n=20 animals control and n>30 animals per RNAi condition. Consistent with its expected function as pathway activator, *smo*(RNAi) enhanced loss of function-phenotypes in combination with the two other pathway activators (A). The fact that gain of function phenotypes caused by *ptc(RNAi)* and *sufu*(RNAi) were also enhanced in combinations with *smo(RNAi)* (B) was an unexpected finding, suggesting that planarian Smo may harbor a cryptic pathway-inhibiting function. The mechanistic basis for this effect is currently unknown. The lack of overt regeneration phenotypes in Cntrl / sufu-mixes was due to the two-fold dilution of the sufu-dsRNA in this experiment. Full-strength *sufu*(RNAi) produces the same range of regeneration phenotypes as *ptc*(RNAi), yet at a somewhat lower penetrance (Sup. Fig. 8). Even though the activation of Hh signaling caused by half strength *sufu*(RNAi) food is presumably below the

threshold for overt regeneration phenotypes, the synergy effects in combination with *ptc(RNAi)* and *smo(RNAi)* indicate that this RNAi-dosage still causes a low level of signal activation.

Figure S11. Temporal requirement of Hh signaling in A/P-specification. Time course of anterior (*sFRP-1*) and posterior (*fz-4*) marker expression at wound sites in **(A)** *Control(RNAi)* **(B)** *hh(RNAi)* **(C)** *ptc(RNAi)* regenerating trunk fragments. Time points are days after amputation. (Phx, Pharynx expression unrelated to regeneration). White arrowheads mark decreased expression relative to control. Black arrowheads mark increased expression relative to control. Scale bars, 0.2 mm. (A) In control animals, both anterior and posterior marker expression progress from scattered expression at 24 h into a dense arc of cells by day 4. (B) In *hh(RNAi)* animals, the posterior is greatly reduced or absent at all time points, but anterior marker expression remains unaffected. (C) In *ptc(RNAi)* animals, anterior marker expression is initiated by 24 hours, but *sFRP-1* positive cells remain scattered and disappear entirely between day 2 and 4. Anterior mis-expression of *fz-4* is already evident by day 2.

Figure S12. (A) Live *APC(RNAi)* animals 14 days after amputation display a similar range of phenotypes as *ptc(RNAi)* animals (Fig. 2, Sup. Fig. 7). Dotted lines, planes of amputation. Scale bar, 0.5 mm. **(B)** *APC(RNAi)* "headless" animals 14 days after amputation, showing lack of anterior marker expression (*sFRP-1*), VNC looping and an ectopic pharynx (arrowhead), both visualized by α-Tubulin antibody staining. Scale bar, 0.5 mm.

Figure S13. (A) *Smed-wnt11-2*-expression in regenerating animals responds to altered Hh- and β-Catenin signaling. *Smed-wnt11-2* expression at anterior and posterior wound sites at d1 and d2 after amputation under indicated RNAi conditions. White arrowheads indicate decreased expression relative to control. Black arrowheads indicate increased expression relative to control. Scale bars, 0.2 mm.

Figure S14. Altered β-Catenin activity does not overtly affect Hh pathway activity. *ptc* expression as indicator of Hh signaling activity at d1 after amputation in RNAi-fed animals. Shorter development of the bottom row was necessary due to the strong upregulation of *ptc* in *sufu(RNAi)* animals. Scale bars, 0.2 mm.

Figure S15. Wnt expression is unaffected by altered Hh signaling in intact animals. **(A)** *wntP-1* expression in the tail of intact RNAi-treated animals. Scale bar, 0.2 mm. **(B)** *Smed-wnt11-2*-expression in uncut RNAi-treated animals.

Figure S16. *ptc* and *hh* expression during regeneration. *ptc* expression (top) or *hh* expression (bottom) in wild type trunk fragments fixed at the indicated time points after amputation. Scale bars, 0.2 mm

Figure S17. Homology analysis of *S.med.* proteins. *S.med.* protein sequences were used to BLAST the *Homo sapiens* (*H.s.*) and *Drosophila melanogaster* (*D.m.*) protein databases. To confirm homology, *D.m.* best hits were used to BLAST the *H.s.* protein database. In cases where forward (f) and reverse (r) sequences of cloned *S.med*. proteins did not overlap, the two sequencing reads were analyzed separately as indicated. Although the top hit for SMED-KIF27 in the *D.m.* protein database was KIF21 and not Cos2, KIF21 is closely related to Cos2 as a member of the Kinesin-4 sub-family (*8*). SMED-KIF27 very likely represents a true Kif27 homolog for the following reasons: A) BLAST of SMED-KIF27 against nr identifies Kif27 homologues from a diverse number of species as top hits, whereas Kif21 homologs score significantly lower. B) The *S.med.* genome contains clear homologs of Kif21A and Kif21B, which likewise BLAST to *Drosophila* Kif21. Thus, this discrepancy is likely an artifact resulting from the comparatively high sequence divergence of SMED-KIF27 and Cos2. The identification of a single planarian

Kif27-homolog supports the notion that vertebrate Kif7 and Kif27 arose by a gene duplication event within the vertebrate lineage (*9*).

Figure S18. Gliding motility in control animals (top) and "inchworming" in absence of cilia (bottom, *IFT172(RNAi)*). Image series obtained from successive movie frames. Dotted yellow line provides a spatial reference to illustrate progress of animal. Scale bar, 2 mm.

Figure S19. Cilia-defective *IFT(RNAi)*-animals regenerate normally. **Top**, single video frame showing normal head (red arrow) and tail (yellow arrow) regeneration 14d after amputation. Scale bar, 1 mm. **Bottom**, Anterior (*sFRP-1*) and posterior (*fz-4*) marker expression in representative trunk fragments from RNAi-fed animals 24 h post amputation. Scale bar: 0.5 mm. *IFT88*- and *IFT52(RNAi)* animals are shown as representative examples of *IFT(RNAi)* phenotypes.

Figure S20. Overtly unaffected *ptc* expression in (A) IFT(RNAi)- animals and (B) *kif27(RNAi)*, *fused(RNAi) or iguana(RNAi)*-animals. Representative examples of non-regenerating RNAi-fed animals are shown. All animals displayed severe "inchworming" at time of fixation. *hh(RNAi)* and *sufu(RNAi)* animals were included as controls for changes in *ptc* expression. Scale bar, 0.5 mm.

Figure S21. *kif27(RNAi)*-, *fused(RNAi)*- and *iguana(RNAi)*-animals regenerate normally. **Top**, Single video frame showing normal head (red arrow) and tail (yellow arrow) regeneration in *kif27(RNAi)*, *fused(RNAi),* and *iguana(RNAi)* animals 14d after amputation. Control, see sup. Fig. 19). Scale bar: 1 mm. **Bottom**, Normal anterior (*sFRP-1*) and posterior (*fz-4*) marker expression in trunk fragments from RNAi-fed animals at 24 h post amputation. Control, see Sup. Fig. 19. Scale bar: 0.5 mm.

Figure S22. *iguana* and *kif27* expression resembles that of cilia associated genes. Gene expression (*in situ* hybridization) in intact animals. Scale bar, 0.5 mm.

Figure S23. Model of Hh pathway evolution. (**Top half)** Summary of differential requirement for cilia and the Cos2/Kif27-Fused complex for Hh signaling in different model systems. Lines between individual elements indicate a functional interconnection. Question marks symbolize lack of experimental data. Iguana functions are explicitly stated. The split of the Kinesin/Fused box into Kif7 and Kif27/Fused in mouse reflects the likely functional specialization of the two murine Cos2 homologues, one for Hh signaling (Kif7) (*10*) and the other for cilia function (Kif27) (*9*). Kif27 function in mammalian cilia biogenesis has not been explicitly demonstrated yet, but appears likely (*9*). The dashed line reflects recent experimental evidence supporting a role for cilia in zebrafish hedgehog signaling (*11*). (**Bottom half)** Likely ancestral state of pathway organization derived from the above data. The dashed line indicates the remaining uncertainty in the ancestral connection between IFT and cilia due to the current lack of experimental association between Hh signaling and cilia in a non-vertebrate organism. However, the connection is probable based on the strongly supported links of Cos2/Kif27-Fused to both Hh signaling and cilia and the role of cilia in the mammalian pathway. According to this model, the separation of the planarian Hh pathway from both cilia and Cos2/Kif27-Fused represents a derived state and phylogenetically basal invertebrates may have retained all three connections.

Movie S1. Control RNAi-treated animals. Behavior of normal body fragments after regeneration. Animals were fed dsRNA against the *C. elegans* gene *unc-22*. Wild type animals were amputated pre- and post-pharyngeally and the resulting fragments allowed to regenerate. Heads and tails regenerated normally in the appropriate anterior and posterior amputation planes. When exposed to light, the animals respond by gliding away from the source using the cilia that covers their ventral surface.

Movie S2. Activation of the Hh signaling pathway. *ptc(RNAi)* trunk fragments regenerate tails at both anterior and posterior amputation planes. The worms are still alive, but both ends attempt to move toward the center of the animal.

Movie S3. Inhibition of *fused.* After pre- and post-pharyngeal amputation, *fused(RNAi)* trunk fragments regenerate heads and tails normally and do not display phenotypes associated with defects in Hh signaling. However, the animals display motility defects ("inchworming" rather than gliding), indicating a role of this molecule in normal cilia functioning.

REFERENCES

1. B. J. Pearson *et al.*, *Dev Dyn* **238**, 443 (Feb, 2009).
2. S. Hunter *et al.*, *Nucleic Acids Res* **37**, D211 (Jan, 2009).
3. K. A. Gurley, J. C. Rink, A. Sánchez Alvarado, *Science* **319**, 323 (Jan 18, 2008).
4. J. Rink, E. Ghigo, Y. Kalaidzidis, M. Zerial, *Cell* **122**, 735 (Sep 9, 2005).
5. C. W. Dunn *et al.*, *Nature* **452**, 745 (Apr 10, 2008).
6. B. J. Pearson, A. Sanchez Alvarado, *Cold Spring Harbor symposia on quantitative biology* **73**, 565 (2008).
7. F. Ronquist, J. P. Huelsenbeck, *Bioinformatics (Oxford, England)* **19**, 1572 (Aug 12, 2003).
8. H. Miki, Y. Okada, N. Hirokawa, *Trends Cell Biol* **15**, 467 (Sep, 2005).
9. C. W. Wilson *et al.*, *Nature* **459**, 98 (May 7, 2009).
10. H. O. Cheung *et al.*, *Sci Signal* **2**, ra29 (2009).
11. P. Aanstad *et al.*, *Curr Biol* **19**, 1034 (Jun 23, 2009).